IAEA
INTERNATIONAL ATOMIC ENERGY AGENCY

20th IAEA Fusion Energy Conference

Vilamoura, Portugal, 1-6 November 2004

IAEA-CN-116 / OV / 1 - 5

Overview of ASDEX Upgrade Results

S. Günter[1], C. Angioni[1], M. Apostoliceanu[1], C. Atanasiu[2], M. Balden[1], G. Becker[1], W. Becker[1], K. Behler[1], K. Behringer[1], A. Bergmann[1], R. Bilato[1], I. Bizyukov[1], V. Bobkov[1], T. Bolzonella[3], D. Borba[4], K. Borrass[1], M. Brambilla[1], F. Braun[1], A. Buhler[1], A. Carlson[1], A. Chankin[1], J. Chen[1], Y. Chen[1], S. Cirant[5], G. Conway[1], D. Coster[1], T. Dannert[1], K. Dimova[1], R. Drube[1], R. Dux[1], T. Eich[1], K. Engelhardt[1], H.-U. Fahrbach[1], U. Fantz[1], L. Fattorini[4], M. Foley[6], P. Franzen[1], J.C. Fuchs[1], J. Gafert[1], K. Gal[7], G. Gantenbein[8], M. García Muñoz[1], O. Gehre[1], A. Geier[1], L. Giannone[1], O. Gruber[1], G. Haas[1], D. Hartmann[1], B. Heger[1], B. Heinemann[1], A. Herrmann[1], J. Hobirk[1], H. Hohenöcker[1], L. Horton[1], M. Huart[1], V. Igochine[1], A. Jacchia[5], M. Jakobi[1], F. Jenko[1], A. Kallenbach[1], S. Kálvin[7], O. Kardaun[1], M. Kaufmann[1], A. Keller[1], A. Kendl[1], M. Kick[1], J.-W. Kim[1], K. Kirov[1], S. Klose[1], R. Kochergov[1], G. Kocsis[7], H. Kollotzek[1], C. Konz[1], W. Kraus[1], K. Krieger[1], T. Kurki-Suonio[9], B. Kurzan[1], K. Lackner[1], P.T. Lang[1], P. Lauber[1], M. Laux[1], F. Leuterer[1], J. Likonen[10], A. Lohs[1], A. Lorenz[1], R. Lorenzini[3], A. Lyssoivan[11], C. Maggi[1], H. Maier[1], K. Mank[1], A. Manini[1], M.-E. Manso[4], P. Mantica[5], M. Maraschek[1], P. Martin[3], K.F. Mast[1], H. Mayer[1], M. Mayer[1], P. McCarthy[6], D. Meisel[1], H. Meister[1], S. Menmuir[13], F. Meo[1], P. Merkel[1], R. Merkel[1], D. Merkl[1], V. Mertens[1], F. Monaco[1], A. Mück[1], H.W. Müller[1], M. Münich[1], H. Murmann[1], Y.-S. Na[1], R. Narayanan[1], G. Neu[1], R. Neu[1], J. Neuhauser[1], D. Nishijima[1], Y. Nishimura[1], J.-M. Noterdaeme[1], I. Nunes[4], M. Pacco-Düchs[1], G. Pautasso[1], A.G. Peeters[1], G. Pereverzev[1], S. Pinches[1], E. Poli[1], T. Pütterich[1], R. Pugno[1], E. Quigley[6], I. Radivojevic[1], G. Raupp[1], M. Reich[1], R. Riedl[1], T. Ribeiro[4], V. Rohde[1], J. Roth[1], F. Ryter[1], S. Saarelma[9], W. Sandmann[1], J. Santos[4], G. Schall[1], H.-B. Schilling[1], J. Schirmer[1], W. Schneider[1], G. Schramm[1], J. Schweinzer[1], S. Schweizer[1], B. Scott[1], U. Seidel[1], F. Serra[4], C. Sihler[1], A. Silva[4], A. Sips[1], E. Speth[1], A. Stäbler[1], K.-H. Steuer[1], J. Stober[1], B. Streibl[1], D. Strintzi[1], E. Strumberger[1], W. Suttrop[1], G. Tardini[1], C. Tichmann[1], W. Treutterer[1], M. Troppmann[1], M. Tsalas[12], H. Urano[1], P. Varela[4], D. Wagner[1], F. Wesner[1], E. Posthumus-Wolfrum[1], E. Würsching[1], M.Y. Ye[1], S.-W. Yoon[1], Q. Yu[1], B. Zaniol[3], D. Zasche[1], T. Zehetbauer[1], H.-P. Zehrfeld[1], M. Zilker[1], H. Zohm[1].

[1]Max-Planck-Institut für Plasmaphysik, EURATOM Association, D-85748 Garching, [2] Institute of Atomic Physics, Romania, EURATOM Association, [3] Consorzio RFX, Padova, Italy, EURATOM Association, [4] Centro de Fusão Nuclear, IST Lisbon, Portugal, EURATOM Association, [5] IFP Milano, Italy, EURATOM Association, [6]

Physics Department, University College Cork, Association EURATOM-DCU, Ireland, [7] KFKI Research Institute, Department of Plasma Physics, Budapest, Hungary, [8] Institut für Plasmaforschung, Stuttgart University, Germany, [9] HUT Helsinki University of Technology, Association EURATOM-Tekes, Espoo, Finland, [10] VTT Technical Research Centre of Finland, Association EURATOM-Tekes, Espoo, [11] Plasma Physics Laboratory, Association “EURATOM-Belgian State”, Belgium, Brussels, [12] Demokritos, Institute of Nuclear Technology, Aghia Paraskevi, Attiki, Greece, [13] KTH- Alba Nora University Centrum, Stockholm, Sweden

Overview of ASDEX Upgrade Results

S. Günter[1], C. Angioni[1], M. Apostoliceanu[1], C. Atanasiu[2], M. Balden[1], G. Becker[1], W. Becker[1], K. Behler[1], K. Behringer[1], A. Bergmann[1], R. Bilato[1], I. Bizyukov[1], V. Bobkov[1], T. Bolzonella[3], D. Borba[4], K. Borrass[1], M. Brambilla[1], F. Braun[1], A. Buhler[1], A. Carlson[1], A. Chankin[1], J. Chen[1], Y. Chen[1], S. Cirant[5], G. Conway[1], D. Coster[1], T. Dannert[1], K. Dimova[1], R. Drube[1], R. Dux[1], T. Eich[1], K. Engelhardt[1], H.-U. Fahrbach[1], U. Fantz[1], L. Fattorini[4], M. Foley[6], P. Franzen[1], J.C. Fuchs[1], J. Gafert[1], K. Gal[7], G. Gantenbein[8], M. García Muñoz[1], O. Gehre[1], A. Geier[1], L. Giannone[1], O. Gruber[1], G. Haas[1], D. Hartmann[1], B. Heger[1], B. Heinemann[1], A. Herrmann[1], J. Hobirk[1], H. Hohenöcker[1], L. Horton[1], M. Huart[1], V. Igochine[1], A. Jacchia[5], M. Jakobi[1], F. Jenko[1], A. Kallenbach[1], S. Kálvin[7], O. Kardaun[1], M. Kaufmann[1], A. Keller[1], A. Kendl[1], M. Kick[1], J.-W. Kim[1], K. Kirov[1], S. Klose[1], R. Kochergov[1], G. Kocsis[7], H. Kollotzek[1], C. Konz[1], W. Kraus[1], K. Krieger[1], T. Kurki-Suonio[9], B. Kurzan[1], K. Lackner[1], P.T. Lang[1], P. Lauber[1], M. Laux[1], F. Leuterer[1], J. Likonen[10], A. Lohs[1], A. Lorenz[1], R. Lorenzini[3], A. Lyssoivan[11], C. Maggi[1], H. Maier[1], K. Mank[1], A. Manini[1], M.-E. Manso[4], P. Mantica[5], M. Maraschek[1], P. Martin[3], K.F. Mast[1], H. Mayer[1], M. Mayer[1], P. McCarthy[6], D. Meisel[1], H. Meister[1], S. Menmuir[13], F. Meo[1], P. Merkel[1], R. Merkel[1], D. Merkl[1], V. Mertens[1], F. Monaco[1], A. Mück[1], H.W. Müller[1], M. Münich[1], H. Murmann[1], Y.-S. Na[1], R. Narayanan[1], G. Neu[1], R. Neu[1], J. Neuhauser[1], D. Nishijima[1], Y. Nishimura[1], J.-M. Noterdaeme[1], I. Nunes[4], M. Pacco-Düchs[1], G. Pautasso[1], A.G. Peeters[1], G. Pereverzev[1], S. Pinches[1], E. Poli[1], T. Pütterich[1], R. Pugno[1], E. Quigley[6], I. Radivojevic[1], G. Raupp[1], M. Reich[1], R. Riedl[1], T. Ribeiro[4], V. Rohde[1], J. Roth[1], F. Ryter[1], S. Saarelma[9], W. Sandmann[1], J. Santos[4], G. Schall[1], H.-B. Schilling[1], J. Schirmer[1], W. Schneider[1], G. Schramm[1], J. Schweinzer[1], S. Schweizer[1], B. Scott[1], U. Seidel[1], F. Serra[4], C. Sihler[1], A. Silva[4], A. Sips[1], E. Speth[1], A. Stäbler[1], K.-H. Steuer[1], J. Stober[1], B. Streibl[1], D. Strintzi[1], E. Strumberger[1], W. Suttrop[1], G. Tardini[1], C. Tichmann[1], W. Treutterer[1], M. Troppmann[1], M. Tsalas[12], H. Urano[1], P. Varela[4], D. Wagner[1], F. Wesner[1], E. Posthumus-Wolfrum[1], E. Würsching[1], M.Y. Ye[1], S.-W. Yoon[1], Q. Yu[1], B. Zaniol[3], D. Zasche[1], T. Zehetbauer[1], H.-P. Zehrfeld[1], M. Zilker[1], H. Zohm[1].

[1]Max-Planck-Institut für Plasmaphysik, EURATOM Association, D-85748 Garching, [2] Institute of Atomic Physics, Romania, EURATOM Association, [3] Consorzio RFX, Padova, Italy, EURATOM Association, [4] Centro de Fusão Nuclear, IST Lisbon, Portugal, EURATOM Association, [5] IFP Milano, Italy, EURATOM Association, [6] Physics Department, University College Cork, Association EURATOM-DCU, Ireland, [7] KFKI Research Institute, Department of Plasma Physics, Budapest, Hungary, [8] Institut für Plasmaforschung, Stuttgart University, Germany, [9] HUT Helsinki University of Technology, Association EURATOM-Tekes, Espoo, Finland, [10] VTT Technical Research Centre of Finland, Association EURATOM-Tekes, Espoo, [11] Plasma Physics Laboratory, Association "EURATOM-Belgian State", Belgium, Brussels, [12] Demokritos, Institute of Nuclear Technology, Aghia Paraskevi, Attiki, Greece, [13] KTH- Alba Nora University Centrum, Stockholm, Sweden

e-mail: Sibylle.Guenter@ipp.mpg.de

Abstract Significant progress has been made on ASDEX Upgrade during the last two years in the basic understanding of transport, in the extension of the improved H-mode in parameter space and towards an integrated operating scenario, and in the development of control methods for major performance limiting instabilities. Highlights were the understanding of particle transport and the control of impurity accumulation based on it, the satisfactory operation with predominantly tungsten-clad walls, the improved H-mode operation over density ranges and for temperature ratios covering the ITER requirements on ν^*, n/n_{GW} and T_e/T_i, the ELM frequency control by pellet injection, and the optimisation of NTM suppression by DC-ECCD through variation of the launching angle. From these experiments an integrated scenario has emerged which extrapolates to a 50 % improvement in $nT\tau$ or a 30 % reduction of the required current compared to the ITER base-line assumptions, with moderately peaked electron and controllable high-Z density profiles.

1. Introduction

During the last two years ASDEX Upgrade has made significant progress in the development and control of attractive operating scenarios for ITER/DEMO and the understanding of the underlying physics. This was made possible by its flexible heating systems (20 MW neutral beam injection with both on- and off-axis heating capability, 5 MW ICRH routinely coupled into H mode plasmas, 2.0 MW ECRH/ECCD allowing for localised heating and current drive), improved diagnostics (see e.g. Sec. 2), and recent extensions of its operating range. These extensions in particular include the prolongation of the flat top time up to 10 s (corresponding to about 5 current diffusion times) and enhanced shaping capabilities ($\delta = 0.55$ for $\kappa \leq 1.7$). Of particular importance for a fusion reactor is the ASDEX Upgrade tungsten programme. Since 1999 ASDEX Upgrade has progressively been increasing its tungsten coverage of the wall surface, especially of those areas identified as net contributors to erosion. The coverage has now reached 65 %, and includes the top divertor target plates and one (sample) low field side protection limiter.

This paper summarises the progress made in the 2003 and 2004 experimental campaigns. The results demonstrate the existence of integrated operating scenarios for ITER with confinement and stability properties well in excess of the ITER baseline scenario. These scenarios were also shown to be compatible with tolerable heat loads to the walls and with high-Z plasma facing components.

2. Consistent model for particle, energy and impurity transport

Concerning the understanding of the energy transport in the plasma core, large progress has been made during the last few years. For prescribed temperatures at the H-mode pedestal top, models based on ITG, TEM and ETG turbulence can quite well reproduce the measured ion and electron temperature profiles [1].

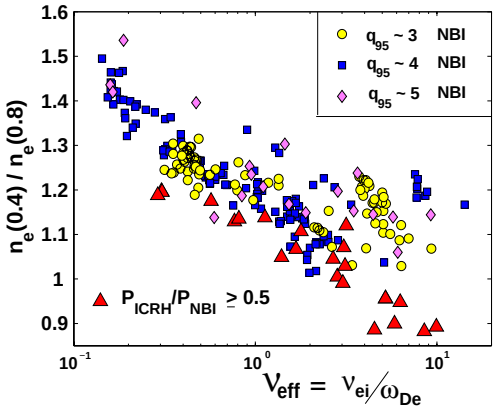

Figure 1: Density peaking, $n_e(\rho_\Psi = 0.4)/n_e(\rho_\Psi = 0.8)$ versus ν_{eff}, $(\rho_\Psi = \sqrt{\Psi/\Psi_{edge}}$, Ψ: poloidal magnetic flux [2].

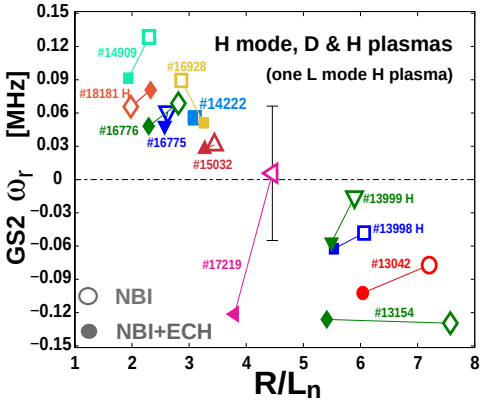

Figure 2: Real frequency of the most unstable mode as a function of R/L_n during NBI phase (open symbols), and NBI + ECH phase (full symbols) [4]

Compared to the usually self-similar temperature profiles, the observed density profiles have a very complex parametric dependence. A general observation in ASDEX Upgrade H-mode as well as L-mode discharges is a reduced density peaking with increasing collisionality [2] (Fig.1). Higher collisionality also leads to a slower time development. Even more complex is the reaction of the density profile to increasing electron heat flux. At low collisionality one observes density flattening, usually termed ”density pump out”. At intermediate collisionalities

($\nu_{eff} = \nu_{ei}/\omega_{De} \approx 1$, ω_{De}: curvature drift frequency) central electron heating even gives rise to a small amount of density peaking, whereas again minor density peaking is observed at high density, see Fig. 2 [3,4].
All these observations are qualitatively consistent with a quasilinear TEM/ITG model, based on either a fluid or a gyro-kinetic description, including dissipative effects [2,4,5]. If the ITG mode is the dominant instability, it causes an anomalous inward pinch at low collisionalities. This inward pinch is considered responsible for the peaked density profiles observed at low collisionality. For higher collisionality this effect vanishes and is replaced by the increasing, but much weaker, neoclassical Ware pinch [2].
Significant electron heating at low collisionality increases the drive for TEMs which are known to cause an outward particle flux. This effect opposes the general trend to peaked density profiles at low collisionality. At medium collisionalities a mixed TEM/ITG regime with small thermodiffusion exists, in which central electron heating (via lowering collisionality, resulting in increased inward pinch) causes density peaking. High collisionality stabilises TEMs so that even strong electron heating does not cause significant changes of the density profile in that case. Based on the model described above one expects moderately peaked density profiles on ITER ($R/L_n \approx 3$) [8]. The electron heat flux and the induced transport were experimentally also shown to have a direct strong influence on impurity transport, making central ECRH/ICRH (and presumably α-particle heating on ITER) an effective tool for impurity control (see Sec. 4).

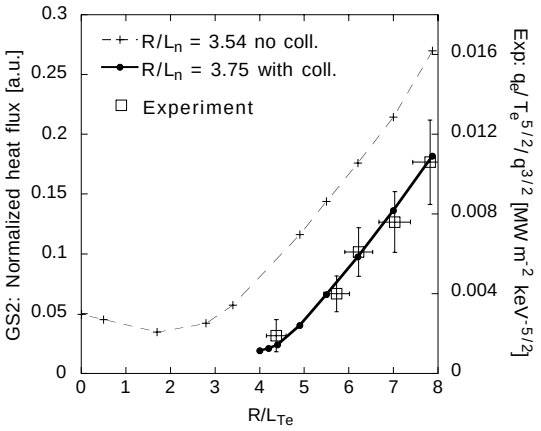

Figure 3: Comparison of the heat flux estimate from GS2 calculations with the measured surface integrated heat flux (for low density, ECRH heated ASDEX Upgrade discharges) [9].

The TEM/ITG model can also explain the measured ion and electron temperature profiles, in particular also features of the response of the latter to modulated electron heating [6,7]. This is demonstrated in Fig. 3, showing a comparison between the calculated quasi-linear and the experimentally observed electron heat fluxes in a low density, ECRH heated ASDEX Upgrade discharge. The critical gradient, the amount of stiffness as well as the collisionality dependence are very well reproduced by the model (note that the saturation level of the turbulence is used as an adjustable parameter, so that only the shape of the curves should be compared) [9].

3. Pedestal physics and ELM control

As it is uncertain whether the benign type II ELM regime previously found on ASDEX Upgrade [10,11] can be transferred to the reactor collisionality regime, we have been alternatively exploring active ELM control regimes. The most successful is the injection of small pellets, each triggering an ELM (”pace making”). The resultant ELMs are reduced in amplitude by the approximate ratio of the imprinted to the ”natural” frequency, with a concomitant confinement reduction much less than if a similar frequency change had been caused by enhanced gas

puffing (Fig. 4) [13,12]. Although the maximum frequency for the pellet injection up to now is limited to about 80 Hz, ELM pace making by pellets is becoming a valuable working tool on the way to an integrated scenario in a carbon free machine, see Sec. 4.

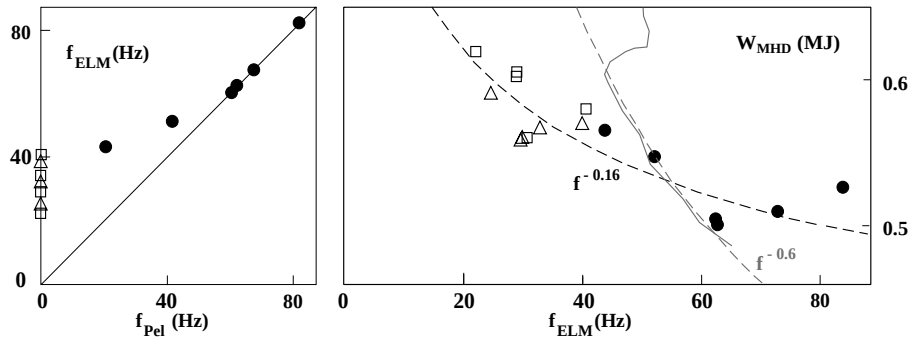

Figure 4: Demonstration of ELM pace making by pellets: ELM frequency vs. pellet frequency (left) and impact on confinement: plasma energy for pellet triggered ELMs (circles) with natural ELMs (squares), and with gas puff increased ELM frequency (triangles) [13,14].

A similar frequency locking of ELMs can be produced also by vertical wobbling of the discharge by a few mm, as pioneered by TCV [15]. As in case of the pellet triggered ELMs, the increase in ELM frequency again causes only a modest confinement reduction [13].
An alternative to the reduction of the ELM size might be the stationary ELM-free "Quiescent H-mode" (QH-mode, first found on DIII-D [16]) which is characterised by good confinement, high pedestal pressure and low pedestal collisionality ($\nu^* < 1$). So far the QH-mode was generally not considered an option for a reactor, owing to the high Z_{eff} values typical for this regime. According to recent studies on ASDEX Upgrade, however, the high value of Z_{eff} does not seem to be an intrinsic property of the QH-mode. A very similar impurity mix was found in low density counter NBI discharges during the QH-mode and ELMy phases. Under optimised machine conditions, QH mode discharges with strongly reduced Z_{eff} values (≈ 2.5) have been realised [17].

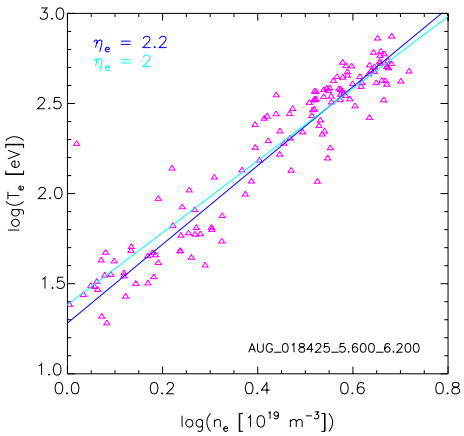

Figure 5: Linear fit of log(electron temperature) vs. log(electron density) in the pedestal region of a type I ELMy H-mode. The best fit gives $\eta_e = 2.2$, $\eta_e = 2.0$ is shown for comparison [18].

Previously QH-mode discharges had also been restricted to very low densities (at low triangularity), as gas puffing usually leads to a rapid transition to an ELMy H-mode. First experiments with pellet fuelling allowed a density increase to about 40 % of the Greenwald limit, without triggering of ELMs by the pellets (in contrast to normal H-modes) [17].
The measurement of the parameters relevant for physics of the H-mode pedestal region and the SOL has been significantly improved by new or refined diagnostic systems. The major improvements are listed below, together with highlights among the achieved results [18].

- *Reflectometry for high temporal and spatial resolution density profile measurements [19,20] and Correlation Doppler reflectometry for the radial electric field, its shear and the correlation length of the density fluctuations [21].* Density profile measurements with high temporal and spatial resolution demonstrated that ELMs are triggered on the LFS,

reaching the HFS after a time delay consistent with the pedestal top ion sound speed [20]. In QH-mode the radial electric field and its shear have been observed to reach twice the value of standard (ELMy) H-modes [22].

- *Li-beam charge exchange for ion edge temperature.* High accuracy H-mode ion temperature measurements showed generally profiles similar to the electron temperatures, albeit with sometimes higher values at the pedestal top [23].

- *Upgrade of the Thomson scattering system [24].* The ratio of the electron density to temperature scale length (η_e) in the pedestal region is found to be very resilient, and approximately 2 in all ASDEX Upgrade H-mode discharges (Fig. 5) [25]. H/D comparison discharges show no correlation of the pedestal width with the neutral penetration length. Snapshots of a two-dimensional edge plasma region show strong, local variations (blobs and holes) during ELMs, both inside and outside the separatrix. From the spacing of these structures one infers toroidal mode numbers of 8 to 20 [18,26].

- *Fast framing infrared camera for the structure of heat deposition.* The power deposition structures observed during type I ELMs are interpreted as footprints of field aligned helical perturbations [27]. From them one derives toroidal mode numbers of 3-5 during the early ELM phase, rising up to 12-14 at the time of maximum power deposition in the divertor [28].

Using the improved diagnostics, the vessel heat load and (volume) radiation pattern has been measured with an ELM relevant time resolution. As shown in [29], the power balance on ASDEX Upgrade (heating power, power into the divertor and radiated power) is satisfied to within 20 % over a wide range of heating power and discharge conditions. The observed heat loads to non-divertor components (caused ,e.g., by ELMs or fast ions), although not significant in the overall power balance (less then 10 %), could become a major concern in a larger device, in particular in combination with high-Z plasma facing components.

4. Tungsten as plasma facing material

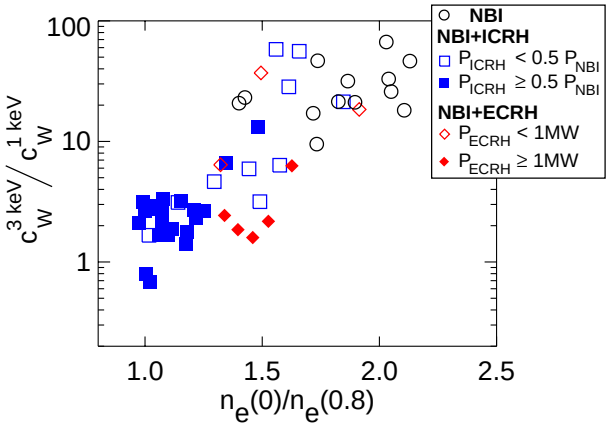

Figure 6: Ratio of central and edge tungsten concentration vs. density peaking for improved H-mode discharges [34].

A future fusion reactor will have to use high-Z materials instead of carbon for all plasma facing components to prevent excessive erosion and to avoid the intolerable high co-deposition of tritium with carbon [30]. (On ASDEX Upgrade the long-term retention of deuterium has been found to be about 3.5 % of the deuterium input [31]). ASDEX Upgrade is developing tungsten as an option by progressive first wall coverage. Since the 19th IAEA conference [32] it has again been substantially increased up to 65 % (24.8 m^2), including in particular those areas known to contribute to net erosion, e.g., the inner heat shield, the upper divertor and one of the guard limiters on the low field side.

Over most operational regimes (including single null operation at the top divertor) the W concentration remains insignificant (below some 10^{-5}). Under certain conditions however, the tungsten concentration rises [33]:

- Compared to an "all carbon" device the difference between limiter and divertor operation is strongly increased. For otherwise similar discharge conditions, the tungsten concentration increased by a factor 100 ($10^{-5} \rightarrow 10^{-3}$) when changing from W divertor to W limiter operation.

- In discharges with low central heating the electron density profiles peak (see Sec. 1), which is followed by (neoclassical) central tungsten accumulation (see, e.g., Fig. 6, [34]).

- In H-mode discharges with prolonged ELM-free phases the tungsten concentration increases over the whole plasma radius, leading to strong radiation losses [35].

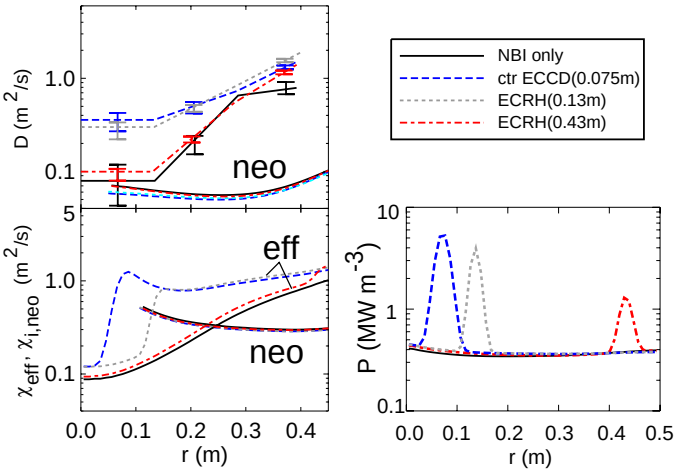

Figure 7: Measured and neoclassical diffusion coefficients (D) of Si, observed and neoclassical ion heat diffusivity (χ) for H-mode discharges on ASDEX Upgrade with NBI heating power of 5 MW, and additional ECRH (0.8 MW) at different radial positions: $r = 0.075\ m, 0.13\ m, 0.43\ m$ [34].

For such conditions, we have developed two successful control strategies: central electron heating (against W peaking) [36] and pellet triggering of ELMs (against W influx) [13]. As discussed in Sec. 1, central electron heating increases the anomalous particle diffusion and is thus an effective tool to reduce the density peaking and the concomitant neoclassical impurity inward pinch. In addition, the increased heat flux directly affects the anomalous impurity diffusion coefficient (Fig. 7) [34].

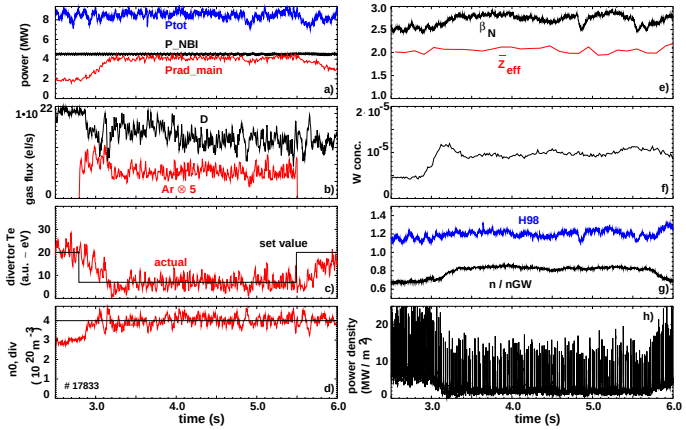

Figure 8: Demonstration of an integrated exhaust scenario: a) heating (4.5 MW NBI, 4 MW ICRH) and main chamber radiated power, b) gas valve fluxes, c) and d) target and measured values of divertor temperature and neutral gas density e) β_N and line averaged Z_{eff} from bremsstrahlung, f) tungsten concentration in the outer central plasma from the W quasi continuum, g) Greenwald fraction and H-factor, f) peak power density in the outer divertor from thermography. The maximum ELM repetition time is set to 25 ms by 40 Hz pellet injection [13].

Due to a strong impurity influx during the inter-ELM phase, the tungsten concentration rises considerably with decreasing ELM frequency. ELM pace making is therefore essential to keep the tungsten concentration low, especially close to the H-L boundary. Its importance will further rise on the way to a full tungsten machine when carbon is missing as the primary intrinsic radiator. In that case, as no extrinsic impurity exists which has the peak of the radiative loss function at comparable low temperatures, the power dissipation will be shifted nearer to the core plasma, reducing the power flow into the pedestal region. For a given heating power, the operating point will therefore be shifted into the low-frequency ELM-regime closer to the H-L threshold.

A successful example of integrated exhaust control is shown in Fig. 8. Here Ar seeding is used to control the divertor temperature. The reduced power flow through the plasma edge would cause a reduction in the type-I ELM frequency leading to a radiative instability and ultimately to a H-L back transition. The situation is stabilised by ELM pace making [13,37].

5. Control of core MHD instabilities

Neoclassical tearing modes have to be either avoided or at least to be kept below a certain amplitude. ASDEX Upgrade has pioneered the technique of active NTM control by ECCD [38,39], and we are further developing this tool. Recently we have investigated the dependence of the suppression efficiency on the ratio of deposition width to island size for DC ECCD. Although the maximum total current drive is expected for large toroidal launching angle, we observe complete island suppression at small launching angles only ($\leq 15^o$, see Fig. 9). In fact, our record β_N/P_{ECCD} achieved with complete NTM suppression (3/2 NTM: β_N = 2.6 for P_{ECCD}=1.0 MW, 2/1 NTM: β_N = 2.3 for P_{ECCD}=1.4 MW) were obtained with a toroidal launching angle of 5^o [40]. This is in accordance with theory as the stabilisation is expected to depend on the current density inside the magnetic island. To reduce the island width well below the ECCD deposition width (a situation of possible relevance for ITER) might therefore require modulated current drive into the island O-point region. In the upcoming campaign we will therefore use our ECCD modulation capability to extend these studies to this operation mode.

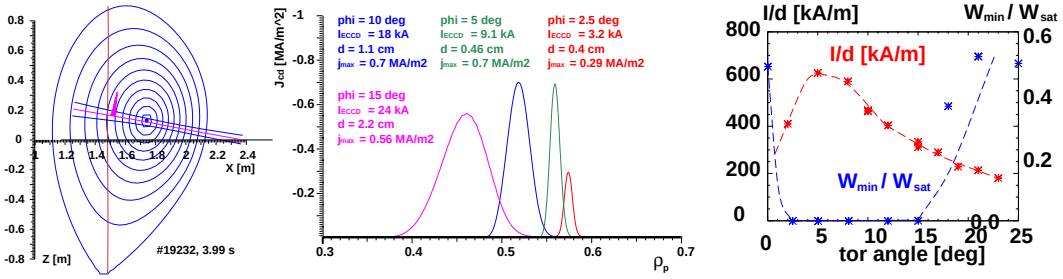

Figure 9: Calculated (TORBEAM) ECCD current profiles for different launching angles at given magnetic field (left). The right figure shows the current normalised to the ECCD deposition width (red) and the ratio of stabilised to "natural" island width (blue) [40].

Beyond certain β_N values, a self-limitation of (3/2) and (4/3) NTM mode activity was discovered on ASDEX Upgrade [41,42]. This phenomenon has been found also on JET at very similar β_N values (see Fig. 10) [43]. Its interpretation in terms of a non-linear mode coupling between the (m,n) NTM, (1,1) mode activity and a (m+1,n+1) pressure driven ideal mode ("FIR-phenomenon") was also verified by active modification of the stability of the latter through current profile tailoring. In accordance with theory this advantageous FIR regime

is favoured by low central magnetic shear (at the $q = 4/3$-surface) as characteristic for the improved H-mode (see Sec. 6).

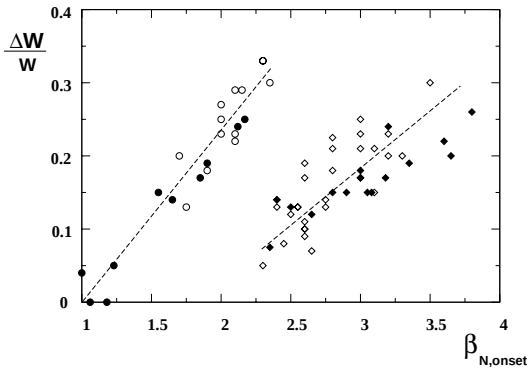

Figure 10: Confinement degradation caused by (3,2) NTMs (energy drop ΔW normalised to plasma energy at the NTM onset W) of saturated NTMs (circles) and FIR-NTMs (diamonds) for ASDEX Upgrade (open symbols) and JET (full symbols) discharges as function of $\beta_{N,onset}$ [43].

The (m,n) = (1,1) activity, usually present in monotonic q-profile scenarios has positive (e.g., impurity control) and negative (e.g., triggering of NTMs, heating efficiency and confinement loss) consequences. We have therefore developed tools for tailoring their amplitude and frequency. Off-axis NBI beam deposition, but in particular co- and counter ECCD, localized around the $q = 1$ surface (as pioneered by TCV [44]), have been shown to provide this on ASDEX Upgrade over a wide range of conditions. As discussed in [40,45], by actively stabilising sawteeth the onset of NTMs has been avoided in discharges otherwise prone to NTMs.
Fast particle driven modes have been investigated in ICRH heated ($P_{ICRH} \geq 2-3$ MW) low density discharges. TAE modes with toroidal mode numbers n=3,4,5,6 are observed with a rather global mode structure, in accordance with MHD calculations [46].

6. Performance improvement beyond the conventional H-mode

The improved H-mode The improved H-mode originally found on ASDEX Upgrade [47] corresponds to H-factor and β_N values projecting to higher Q and/or longer pulse length for ITER than the standard scenario. It is now viewed as the prime candidate for hybrid scenarios on ITER. This regime is characterised by q-profiles with low central magnetic shear and $q_0 \geq 1$. As in standard H-mode, the temperature profiles are self-similar, but the density profiles are peaked. The absence of sawteeth increases the threshold for NTM onset. Even at high β_N values the (4,3) and (3,2) NTM activity remains benign (for $q_0 \approx 1$ this is supported by the FIR character of the modes) [43]. The stability limit is given by the onset of (2,1) NTMs at $\beta_N > 3$ (the actual value depending on collisionality and q_{95}). The regime has been shown to be compatible with type II ELMs as well as high Z walls (with central electron heating to avoid impurity accumulation) [48].
In recent experiments we verified the existence of this regime in scans over the full range of ρ^* allowed by the operating capabilities of our device (from I_p/B_t = 0.6 MA/1.4 T up to 1.2 MA/2.8 T) at either constant collisionality or constant Greenwald fraction, and at high β_N [49]. A summary of the performance obtained in terms of fusion gain ($H_{98(y,2)}\beta_N/q_{95}^2$) vs. a measure proportional to the bootstrap current ($\sqrt{\varepsilon}\beta_p$) is given in Fig. 11. For all q_{95} values shown, stationary long pulses (duration $> 40\tau_E$) were obtained with close to maximum performance, limited only by technical constraints. The figure of merit describing the fusion gain achieved at $q_{95} \sim 3-3.5$ ($H_{98(y,2)}\beta_N/q_{95}^2 \sim 0.3$) exceeds the ITER baseline scenario by about 50 %. Thus the ITER performance is achieved already for $q_{95} = 4$, allowing for longer pulses due to the reduced plasma current, with a high bootstrap current fraction (e.g., with a total non-inductive current fraction of 50 % achieved with $q_{95} = 3.6$). In terms of dimensionless parameters, the ITER collisionality ν^* is reached in the low density discharges. The normalised

Lamor radii ρ^* achieved on ASDEX Upgrade are, of course, still well above the ITER value. The range of ρ^* covered is, however, being further extended in a joint effort of various devices [50].

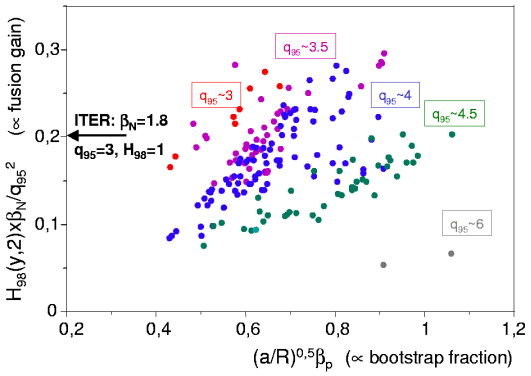

Figure 11: $H_{98(y,2)}\beta_N/q_{95}^2$ (proportional to fusion gain) vs. $\sqrt{\varepsilon}\beta_p$ (proportional to bootstrap current fraction) for improved H-mode discharges on ASDEX Upgrade at various values of q_{95}. For comparison the ITER reference value for the baseline scenario is given [49].

Although in most experiments the improved H-mode has been reached with dominant NBI heating resulting in $T_i > T_e$, the latter condition is not essential for the improved confinement. Recent experiments on ASDEX Upgrade with significant electron heating have verified the existence of this high confinement regime for $T_i = T_e$ as well.

NBI current profile control To achieve a steady state scenario with reversed magnetic shear, means for current profile control are required. For ITER, off-axis current drive by negative ion based NBI (N-NBI) is envisaged. Beam drive of current has been predicted by theory (see e.g. [51]) and observed in many experiments (e.g., in TFTR [52], DIII-D [53], JET [54], JT-60U [56]). In most of these experiments the beam driven current was located on-axis, including those with N-NBI ([56]). The only off-axis current drive (with 2 MW NBI power) has been reported by JT-60U [55].

In order to facilitate current profile control by off-axis NBI, ASDEX Upgrade has reoriented one of its beam boxes towards a more tangential injection [57]. Although in early experiments significant differences between the loop voltages in discharge phases with on-axis heating and off-axis current drive have been found, no evidence of changes in the current profile was observed, in marked contrast to predictions of the ASTRA transport code [58]. Recently more detailed experiments were performed, investigating the current drive efficiency for different discharge conditions. It was found that the amount of driven current strongly depends on the total heating power.

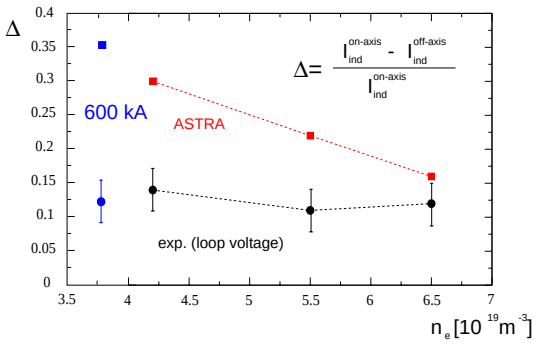

Figure 12: Comparison of the predicted (red) and measured (black) relative changes in the current driven by the Ohmic transformer between discharge phases of on- and off-axis NBI. Discharge conditions: $B_t = 2.5T, I_p = 800(600)kA, \delta = 0.15, P_{NBI} = 5MW$ [59].

Above a certain NBI power (low δ : $P_{NBI} > 3$ MW, high δ : $P_{NBI} \geq 5$ MW) the current drive efficiency derived from the loop voltage was well below the value predicted by the ASTRA code (see, e.g., Fig. 12 for a comparison between observed and predicted current for $\delta = 0.15, P_{NBI} =$ 5 MW). Although even at these reduced efficiencies, the remaining NBI current drive (e.g., ≥ 100 kA for $n_e = 4 \cdot 10^{19}$) should still give rise to significant current profile modifications, no

changes in the current profile were observed (MSE, location of MHD modes).
Current profile modifications, largely consistent with ASTRA-code simulations, were however observed for low heating powers [59]. Fig 13 shows that the predicted current profile relaxation, after switching from off-axis to on-axis beams, is in quite good agreement with the MSE measurements. In particular, the anticipated amount of beam current appears to be driven (albeit localised at smaller radii than calculated by ASTRA). The corresponding modification of the q-profile is also consistent with the shift of the $q = 1.5$ surface determined from a small (3,2) NTM in this particular discharge.

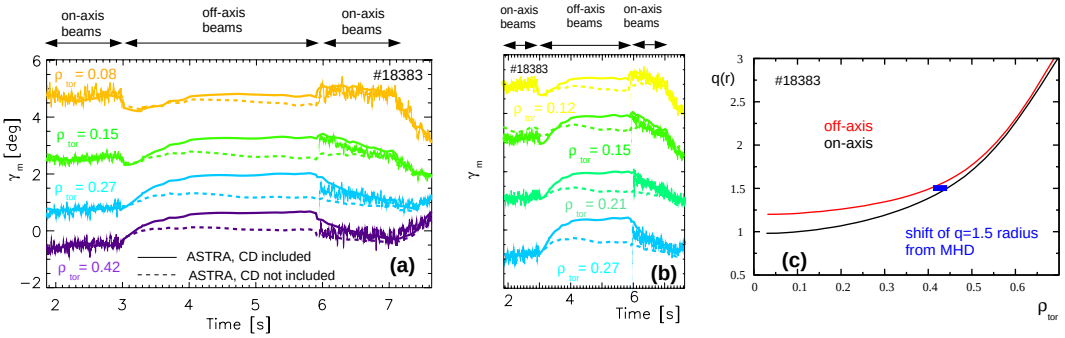

Figure 13: Time traces of the MSE signal during the on-axis phase compared to ASTRA predictions including (solid line) and excluding (dashed line) the beam current contribution (a,b), and comparison of q profiles between discharge phases with on- and off-axis NBI (c). The q-profile modification is consistent with the shift of the $q = 1.5$ surface as derived from the location of the (3,2) MHD activity. $B_t = 2.5T, I_p = 800kA, \delta = 0.4, P_{NBI} = 5MW$ [59].

Dedicated experiments have been performed to investigate a possible influence of MHD or fast particle driven modes: Discharges at different q_{95} (between 4.0 and 6.2), excluding in particular a $q = 1$ surface ($q_{95} > 6$), and the frequent absence of measurable MHD activity exclude a dynamo-type re-arrangement of the magnetic field. Any influence of fast particle resonant modes (which were not observed in any of these experiments) has been ruled out by varying spatial and pitch angle distribution of the beam ions as well as their energy. At comparable heating power the results were virtually identical also for a reduced beam voltage (69 kV) ensuring the deuterium ion velocity to be below the Alfvén resonance at $v_A/3$.
The results described above indicate a diffusive redistribution of fast ions, driven by turbulent fluctuations correlated with the thermal transport. Such a redistribution would fill in the fast particle distribution in the centre, but would also bring energetic ions into the outer, cooler regions, where they would undergo a faster slowing-down, resulting in an overall reduced current drive efficiency. It should be noted that this spreading would have a much smaller effect on other measures of the fast ion population, like their β contribution or the neutron production, as the latter effects weight more strongly the highest velocity phase of the slowing down history. Our experiments do not contradict earlier experiments reporting classical fast particle slowing behaviour (see, eg., [60]) either as all these experiments were done at very low total heating power.

7. Summary and Outlook

The experimental effort of ASDEX Upgrade is mainly focussed on the development of a consistent high performance scenario for ITER, and of a suite of control tools to access and stabilise this and other favourable operating regimes. During the last two years we have demonstrated the robustness of our "improved H-mode", which now forms the basis of the long pulse ITER hybrid scenarios, establishing it over a broad range of conditions: densities ranging from $n = n_{GW}$ down

to values corresponding to the ITER collisionality, heating scenarios which achieve $T_e = T_i$, q_{95} values down to 3, β_N values of at least 3 (with only benign MHD-activity), bootstrap fractions up to 50 %, and the ρ^* range accessible within a factor of 2 variation in B_t and I_p. All results were obtained with a predominantly W-clad first wall (65 % coverage) without performance-affecting impurity influx. At near-Greenwald densities these discharges show well-tolerable type-II ELMs. The maximum performance parameters obtained would allow ITER operation either at 50 % increased $H_{98(y,2)}\beta_N/q_{95}^2(\sim Q)$, or at 30 % reduced plasma current.

For active control of discharges we have refined our diagnostic systems (particularly in the plasma edge region), improved the physics understanding (particularly of particle transport) and developed suitable actuators. In the presence of high-Z plasma facing components both the influx of impurities through the edge barrier and their central peaking has to be avoided. The former has been achieved by ELM control through pellet pace-making. Central electron heating was found effective to counteract impurity accumulation by affecting plasma density profiles and impurity diffusion. In the area of direct NTM control we have optimised the efficiency of stabilisation by DC-ECCD through variation of the launching angle and increased thereby the stabilised β_N. ECCD was also successfully employed to control sawteeth, in particular to avoid NTM seeding.

In the near future we will progressively complete the tungsten cladding of the first walls. For the upcoming campaign we will cover mainly the guard limiters and (as prototype) one ICRH limiter on the low field side. The pellet ELM-triggering capability will be extended to higher frequencies and smaller pellets by a new blower gun. ECCD for NTM stabilisation should become a working tool owing to new steerable mirrors for resonant surface tracking and the enhancement of power by additional gyrotrons with a multi-frequency capability.

References

[1] TARDINI, G. et al., Nucl. Fusion **42** (2002) 258.
[2] ANGIONI, C. et al., Phys. Rev. Lett. **90** (2003) 205003.
[3] STOBER, J. et al., Nucl. Fusion **41** (2001) 1535.
[4] ANGIONI, C. et al., Nucl. Fusion **44** (2004) 827.
[5] PEETERS, A. et al., this conference, IAEA-CN-116/EX/P3-10.
[6] RYTER, F. et al., Nucl. Fusion **43** (2003) 1396.
[7] JACCHIA, A. et al., this conference, IAEA-CN-116/EX-P-6/17 this conference, IAEA-CN-116/EX/P3-10..
[8] PEREVERZEV, G.et al., Theoretical predictions of the density profile in a tokamak reactor, submitted to Nucl. Fusion, 2004.
[9] PEETERS, A. G.et al., Linear gyro-kinetic stability calculations of electron heat dominated plasmas in ASDEX Upgrade, submitted to Phys. Plasmas, 2004.
[10] GRUBER, O. et al., Tolerable ELMs in conventional and advanced scenarios at ASDEX Upgrade, 19th IAEA Conference Fusion Energy, Lyon, France, October 2002, IAEA–CN–94/EX/C2–1
[11] STOBER, J. et al., Nucl. Fusion **41** (2001) 1123.
[12] LANG, P. et al., Nucl. Fusion **44** (2004) 665.
[13] LANG, P. T. et al., this conference, IAEA-CN-116/EX-2/6.
[14] LANG, P. et al., Plasma Phys. Controlled Fusion **46** (2004) L31.
[15] DEGELING, A. W.et al., Plasma Phys. Controlled Fusion **45** (2003) 1637.
[16] BURRELL, K. H.et al., Plasma Phys. Controlled Fusion **44** (2002) A253.
[17] SUTTROP, W. A. et al., this conference, IAEA-CN-116/EX-4/5.
[18] HORTON, L. D. et al., this conference , IAEA-CN-116/EX-P-3/4.
[19] NUNES, I. et al., this conference, IAEA-CN-116/EX-P-6/20.
[20] NUNES, I. et al., Nucl. Fusion **44** (2004) 883.
[21] CONWAY, G. D. et al., Plasma Phys. Controlled Fusion **46** (2004) 951.

[22] SCHIRMER, J.et al., Radial electric field shear and correlation length measurements on ASDEX Upgrade using correlation Doppler refectometry, 31th EPS Conference on Plasma Physics and Controlled Fusion, London, 2004, P–4.127.
[23] REICH, M.et al., Plasma Phys. Controlled Fusion **46** (2004) 797.
[24] KURZAN, B. et al., Plasma Phys. Controlled Fusion **46** (2004) 299.
[25] NEUHAUSER, J.et al., Plasma Phys. Controlled Fusion **44** (2004) 855.
[26] KURZAN, B.et al., Evidence for blobs and holes of electron density and temparture during type I edge localised modes in ASDEX Upgrade, submitted to Phys. Rev. Lett., 2004.
[27] EICH, T. et al., Phys. Rev. Lett. **91** (2003) 195003.
[28] EICH, T. et al., Type I ELM substructure on the divertor target plates in ASDEX Upgrade, submitted to Plasma Phys. Controlled Fusion, 2004.
[29] HERRMANN, A. et al., this conference, IAEA-CN-116/EX-2/4b.
[30] BOLT, H.et al., J. Nucl. Matter **329-333** (2004) 66.
[31] MAYER, M. et al., this conference, IAEA-CN-116/EX-P-5/24.
[32] ROHDE, V. et al., 19th IAEA Conference Fusion Energy, Lyon, France, October 2002, IAEA–CN–94/EX/D1-4
[33] NEU, R. et al., this conference, IAEA-CN-116/EX-10/5.
[34] DUX, R. et al., this conference, IAEA-CN-116/EX-P-6/14.
[35] DUX, R., Fusion Science and Technology **44** (2003) 708.
[36] NEU, R. et al., Plasma Phys. Controlled Fusion **44** (2002) 1021.
[37] KALLENBACH, A. et al., Integrated exhaust control with divertor parameter feedback and pellet ELM pacemaking in ASDEX Upgrade submitted to Journal Nucl. Mat, 2004
[38] ZOHM, H. et al., Nucl. Fusion **39** (1999) 577.
[39] GANTENBEIN, G. et al., Phys. Rev. Lett. **85** (2000) 1242.
[40] MARASCHEK, M. et al., this conference, IAEA-CN-116/EX-7/2.
[41] GUDE, A. et al., Nucl. Fusion **42** (2002) 833.
[42] GÜNTER, S. et al., Phys. Rev. Lett. **87** (2001) 275001.
[43] GÜNTER, S. et al., Nucl. Fusion **44** (2004) 524.
[44] ANGIONI, C.et al., Nucl. Fusion **43** (2003) 455.
[45] MÜCK, A. et al., NTM control via sawtooth tailoring in ASDEX Upgrade, 30th EPS Conference on Controlled Fusion and Plasma Physics, St. Petersburg, 2003, P–1.131.
[46] BORBA, D. et al., this conference, IAEA-CN-116/EX-P-4/37.
[47] GRUBER, O. et al., Phys. Rev. Lett. **83** (1999) 1787.
[48] SIPS, A. C. C. et al., Plasma Phys. Controlled Fusion **44** (2002) A151.
[49] STÄBLER, A. et al., this conference, IAEA-CN-116/EX-4/5.
[50] SIPS, A. C. C. et al., this conference, IAEA-CN-116/IT-P-3/36.
[51] CORDEY, J. G. et al., Nucl. Fusion **19** (1979) 249.
[52] ZARNSTORFF, M. C. et al., Phys. Rev. Lett. **60** (1988) 1306.
[53] FOREST, C. B.et al., Phys. Rev. Lett. **73** (1994) 2444.
[54] CHALLIS, C. D. et al., Nucl. Fusion **29** (1989) 563.
[55] IDE, S. et al., Non-inductive current drive experiments for profile control in JT-60U, Proc. 15th IAEA Conference, Seville, 1994, IAEA-CN-60/A-5-I-4.
[56] OIKAWA, T. et al., Nucl. Fusion **41** (2001) 1575.
[57] STÄBLER, A. et al., Fusion Science and Technology **44** (2003) 730.
[58] HOBIRK, J. et al., Off-axis neutral beam current drive experiments on ASDEX Upgrade and JT-60U, 30th EPS Conference on Controlled Fusion and Plasma Physics, St. Petersburg, O–4.1B.
[59] GÜNTER, S.et al., Conditions for NBI current profile control on ASDEX Upgrade, 31th EPS Conference on Plasma Physics and Controlled Fusion, London, 2004, O1–02.
[60] EFTHIMION, P. C. et al., Transport studies on TFTR utilizing perturbation techniques, page 307, Proc. 12th IAEA Fusion Energy Conference, Nice, 1988.